Wide-Angle Absorbing Boundary Conditions for Low and High-Order FDTD Algorithms

Mohammed F. Hadi

Electrical Engineering Dept., Kuwait University, P. O. Box 5969, Safat 13060, Kuwait

Abstract – Wide-angle performance of the perfectly-matched-layer absorbing boundary conditions for the finite-difference time-domain (FDTD) method is investigated for efficient modeling of electrically large structures. The original split-field, uniaxial and convolutional perfectly-matched-layer formulations are all optimized to produce near-flat absorption for incidence angles up to 87 degrees. Optimized wide-angle parameters are derived for both the standard FDTD method and a high-order finite-volumes-based variant. The investigated high-order algorithm in particular is shown to produce improved wide-angle performance over standard FDTD for all three perfectly-matched-layer variants even when they are optimized for normal wave incidence. In all cases, optimization is managed through appropriate choices of modeling parameters which can be directly and unobtrusively applied to existing FDTD codes.

Keywords: FDTD methods, PML absorbing boundary conditions, high-order methods, electrically large structures.

I. INTRODUCTION

With the recently mounting interest in Giga-Hertz and Tera-Hertz communications systems and devices, modeling electrically large structures is fast becoming a pressing need for designers and installers of those systems. The finite-difference time-domain (FDTD) method, especially in its high-order forms [1–11], is capable of accurately and efficiently modeling such large structures provided that the various FDTD modeling tools are updated to match their high accuracy [12–14]. One of those tools is the ability to truncate unbounded spaces with efficient absorbing boundary conditions. The current state of the art in this area is Bérenger's perfectly-matched-layer (PML) which comes in several different implementations [15–20]. Modeling electrically large problems presents a real challenge in this regard due to the large interface areas between the modeled structure and its surrounding absorbing layers. Such extended interfaces cause appreciably large outgoing energies to impinge on absorbing layers at steep angles where PML absorbing abilities quickly diminish [21]. This problem is exacerbated with the relatively coarse FDTD grids allowed by the high-order algorithms

and demanded by computational efficiency requirements when modeling electrically large structures.

Several works investigated approaches to optimize PML parameters for maximum wide-angle absorption [22–26]. Most of these works were concerned with achieving maximum absorption for the incidence angles range of $0 \leq \theta \leq 75°$ (with $\theta = 0$ representing normal incidence). While this operating range is reasonably unrestrictive when designing PML for electrically small FDTD models, it is not sufficient for electrically large modeling purposes. The moderately large two-dimensional building model investigated in [2], for example, had to be increased in size three-fold to insure adherence to a $75°$ incidence angle limit on all outgoing waves impinging on the surrounding PML region. Clearly, extending the PML operating range to near grazing incidence angles is critical for efficient electrically large FDTD models. One effort that pushed PML wide-angle functionality beyond $\theta = 75°$ is the work of Kantartzis, Yioultsis, Kosmanis and Tsiboukis [26] which introduced a non-diagonally anisotropic PML where all nine dielectric tensor's elements are nonzero. This approach demonstrated good wide-angle PML performance at the expense of some mathematical complexity and added computational overhead.

It will be demonstrated in this work that the three major PML variants– the original split-field PML [15], the uniaxial PML [17, 18] and the convolutional PML [19, 20]– are all capable of near-flat absorption response for the incidence angles range of $0 \leq \theta \leq 87°$. This very useful extended range will be realized through optimization routines that utilize complete FDTD/PML codes as functional arguments and PML parameters as optimization variables. Furthermore, this wide-angle capability will be demonstrated for both the standard FDTD method and a recently-developed finite-volumes-based algorithm [11] as a representative of high-order FDTD methods. Most critically, this wide-angle functionality does not require changes to existing FDTD/PML codes or result in added computational overhead.

II. FDTD AND PML FORMULATIONS

The various simulations and optimization analysis in this work will be based on the following FDTD and PML

implementations, with the E_x field update equations as representative samples.

A. Split-Field PML Formulation

For this original PML formulation, the $E_x = E_{xy} + E_{xz}$ update equation is given by [15],

$$
\begin{aligned}
E_{xy}|^{n+\frac{1}{2}} &= e^{-\sigma_y \Delta t/\epsilon} \, E_{xy}|^{n-\frac{1}{2}} + \\
&\quad \frac{1 - e^{-\sigma_y \Delta t/\epsilon}}{\sigma_y} \, D_y H_z
\end{aligned} \tag{1}
$$

$$
\begin{aligned}
E_{xz}|^{n+\frac{1}{2}} &= e^{-\sigma_z \Delta t/\epsilon} \, E_{xz}|^{n-\frac{1}{2}} - \\
&\quad \frac{1 - e^{-\sigma_z \Delta t/\epsilon}}{\sigma_z} \, D_z H_y,
\end{aligned} \tag{2}
$$

where the PML loss profile is coded by Holland's exponential time-stepping formula [27]. For the standard FDTD method, the $D_y H_z$ and $D_z H_y$ difference operators refer to,

$$
D_y H_z = \frac{1}{h} \left[H_z|_{j+\frac{1}{2}} - H_z|_{j-\frac{1}{2}} \right] \tag{3}
$$

$$
D_z H_y = \frac{1}{h} \left[H_y|_{k+\frac{1}{2}} - H_y|_{k-\frac{1}{2}} \right], \tag{4}
$$

where the non-staggered i, j, k and n spatial and temporal indices are omitted for cleaner notation. The spatial difference operators for the high-order algorithm are represented by [11],

$$
\begin{aligned}
D_y H_z = &\; \frac{K_a}{h} \left[H_z|_{j+\frac{1}{2}} - H_z|_{j-\frac{1}{2}} \right] + \\
&\; \frac{K_b}{3h} \left[H_z|_{j+\frac{3}{2}} - H_z|_{j-\frac{3}{2}} \right] + \\
&\; \frac{K_c}{12h} \begin{bmatrix} H_z|_{i+1,j+\frac{3}{2}} + H_z|_{i-1,j+\frac{3}{2}} \\ +H_z|_{j+\frac{3}{2},k+1} + H_z|_{j+\frac{3}{2},k-1} \\ -H_z|_{i+1,j-\frac{3}{2}} - H_z|_{i-1,j-\frac{3}{2}} \\ -H_z|_{j-\frac{3}{2},k+1} - H_z|_{j-\frac{3}{2},k-1} \end{bmatrix} + \\
&\; \frac{K_d}{12h} \begin{bmatrix} H_z|_{i+1,j+\frac{3}{2},k+1} + H_z|_{i-1,j+\frac{3}{2},k+1} \\ +H_z|_{i+1,j+\frac{3}{2},k-1} + H_z|_{i-1,j+\frac{3}{2},k-1} \\ -H_z|_{i+1,j-\frac{3}{2},k+1} - H_z|_{i-1,j-\frac{3}{2},k+1} \\ -H_z|_{i+1,j-\frac{3}{2},k-1} - H_z|_{i-1,j-\frac{3}{2},k-1} \end{bmatrix}
\end{aligned} \tag{5}
$$

and

$$
\begin{aligned}
D_z H_y = &\; \frac{K_a}{h} \left[H_y|_{k+\frac{1}{2}} - H_y|_{k-\frac{1}{2}} \right] + \\
&\; \frac{K_b}{3h} \left[H_y|_{k+\frac{3}{2}} - H_y|_{k-\frac{3}{2}} \right] + \\
&\; \frac{K_c}{12h} \begin{bmatrix} H_y|_{i+1,k+\frac{3}{2}} + H_y|_{i-1,k+\frac{3}{2}} \\ +H_y|_{j+1,k+\frac{3}{2}} + H_y|_{j-1,k+\frac{3}{2}} \\ -H_y|_{i+1,k-\frac{3}{2}} - H_y|_{i-1,k-\frac{3}{2}} \\ -H_y|_{j+1,k-\frac{3}{2}} - H_y|_{j-1,k-\frac{3}{2}} \end{bmatrix} + \\
&\; \frac{K_d}{12h} \begin{bmatrix} H_y|_{i+1,j+1,k+\frac{3}{2}} + H_y|_{i-1,j+1,k+\frac{3}{2}} \\ +H_y|_{i+1,j-1,k+\frac{3}{2}} + H_y|_{i-1,j-1,k+\frac{3}{2}} \\ -H_y|_{i+1,j+1,k-\frac{3}{2}} - H_y|_{i-1,j+1,k-\frac{3}{2}} \\ -H_y|_{i+1,j-1,k-\frac{3}{2}} - H_y|_{i-1,j-1,k-\frac{3}{2}} \end{bmatrix}.
\end{aligned} \tag{6}
$$

An explanation and derivation procedure for the K tuning parameters in the above equations, which play a key role in minimizing numerical dispersion errors, can be found in [11].

Due to the extended reach of the high-order update equations (up to $\pm 3h/2$ from the updated field node), special difference operators are required for the FDTD layers bordering the PML's perfect-electric-conductor back-planes [13]. For example, when the E_x node is adjacent to a planar conducting boundary normal to the x-axis, the difference operators (5) and (6) reduce to,

$$
\begin{aligned}
D_y H_z = &\; \frac{K_a^b}{h} \left[H_z|_{j+\frac{1}{2}} - H_z|_{j-\frac{1}{2}} \right] + \\
&\; \frac{K_b^b}{3h} \left[H_z|_{j+\frac{3}{2}} - H_z|_{j-\frac{3}{2}} \right] + \\
&\; \frac{K_c^b}{6h} \begin{bmatrix} H_z|_{j+\frac{3}{2},k+1} + H_z|_{j+\frac{3}{2},k-1} \\ -H_z|_{j-\frac{3}{2},k+1} - H_z|_{j-\frac{3}{2},k-1} \end{bmatrix}
\end{aligned} \tag{7}
$$

$$
\begin{aligned}
D_z H_y = &\; \frac{K_a^b}{h} \left[H_y|_{k+\frac{1}{2}} - H_y|_{k-\frac{1}{2}} \right] + \\
&\; \frac{K_b^b}{3h} \left[H_y|_{k+\frac{3}{2}} - H_y|_{k-\frac{3}{2}} \right] + \\
&\; \frac{K_c^b}{6h} \begin{bmatrix} H_y|_{j+1,k+\frac{3}{2}} + H_y|_{j-1,k+\frac{3}{2}} \\ -H_y|_{j+1,k-\frac{3}{2}} - H_y|_{j-1,k-\frac{3}{2}} \end{bmatrix}.
\end{aligned} \tag{8}
$$

Readers are referred to [13] for more difference operators adjustments that deal with other conductor proximity situations as well as explanation of the above K-parameters and their relations to those in equations (5) and (6). Interested readers in the two-dimensional version of this high-order algorithm [2] can find similar treatments in [12].

B. Uniaxial and Convolutional PML Formulations

For these PML variants, Roden and Gedney's update equations will be used [20],

$$
E_x|^{n+\frac{1}{2}} = E_x|^{n-\frac{1}{2}} + \frac{\Delta t}{\epsilon} \begin{bmatrix} D_y H_z/\kappa_y + \psi_y \\ -D_z H_y/\kappa_z - \psi_z \end{bmatrix} \tag{9}
$$

where the difference operators for both FDTD algorithms are the same ones given in equations (3) and (6), and,

$$
\psi_y = b_y \psi_y|^{n-1} + c_y D_y H_z \tag{10}
$$

$$
\psi_z = b_z \psi_z|^{n-1} + c_z D_z H_y, \tag{11}
$$

with

$$
b_y = \exp\left[-\left(\frac{\sigma_y}{\epsilon \kappa_y} + \frac{a_y}{\epsilon} \right) \right] \tag{12}
$$

$$
b_z = \exp\left[-\left(\frac{\sigma_z}{\epsilon \kappa_z} + \frac{a_z}{\epsilon} \right) \right], \tag{13}
$$

$$
c_y = \frac{(b_y - 1)\sigma_y/\kappa_y}{\sigma_y + \kappa_y a_y}, \tag{14}
$$

$$
c_z = \frac{(b_z - 1)\sigma_z/\kappa_z}{\sigma_z + \kappa_z a_z}. \tag{15}
$$

The above equations fully describe the convolutional PML formulation, whereas the special case uniaxial PML formulation is realized by setting $\kappa_{y,z} = 1$ and $a_{y,z} = 0$ [18].

C. PML Loss Profiles

The three PML parameters, σ, κ and a, will be coded with the polynomial profiles,

$$\sigma(\rho) = \sigma_{\max} \left(\frac{\rho}{d}\right)^{n_\sigma} \tag{16}$$

$$\kappa(\rho) = 1 + (\kappa_{\max} - 1)\left(\frac{\rho}{d}\right)^{n_\kappa}, \tag{17}$$

$$a(\rho) = a_{\max} \left(\frac{d - \rho}{d}\right)^{n_a}, \tag{18}$$

where ρ is the incremental PML depth measured from its interface with the scatterer region and d is the PML thickness. PML optimization and performance will now be decided based on proper choices of three parameters ($\sigma_{\max}$, n_σ and d) for the split-field and uniaxial PML and seven parameters ($\sigma_{\max}$, n_σ, $\kappa_{\max}$, n_κ, $a_{\max}$, n_a and d) for the convolutional PML. For the following analysis, one deviation from the literature should be mentioned here. The $\kappa \geq 1$ constraint [20, 28] will be relaxed to $\kappa \geq 0$. This step will prove to be crucial for realizing optimum wide-angle convolutional PML profiles as will become obvious in Section IV.

III. PML OPTIMIZATION PROCEDURE

For each of the three PML variants, optimum profiles were determined using MATLAB's FMINSEARCH optimization routine. This routine was set up to minimize an error quantity (Ψ) which is the maximum difference of two E_z surface plots from two FDTD simulations; one incorporating the PML formulation under study while the other is a large reference three dimensional space with matching FDTD parameters. The test domain is a $50 \times 50 \times 51$-cell vacuum terminated by a 10-layer PML (see Fig. 1). An E_z hard point-source [15] is introduced at the center of the vacuum that is non-zero only for the duration $0 \leq \omega t \leq 2\pi$,

$$E_z = \frac{1}{32} \left[10 - 15\cos(\omega t) + 6\cos(2\omega t) - \cos(3\omega t)\right]. \tag{19}$$

The chosen first harmonic of this signal is 1 GHz and the uniform FDTD grid size in all three dimensions is set as $h = \lambda/20$ at this frequency. The time step is set as the maximum allowed by each algorithm's stability criterion. The simulation time is chosen to be long enough to allow appropriate interaction of the outgoing wave with the PML interface, inner layers and backplanes; 100 and 110 times steps for standard and high-order FDTD, respectively. For the standard FDTD simulations, for instance, Fig. 2 shows that the lead propagating peak reaches the PML interface at time step $n = 53$. It also reaches the backplane of the 10-layer PML at $n = 74$
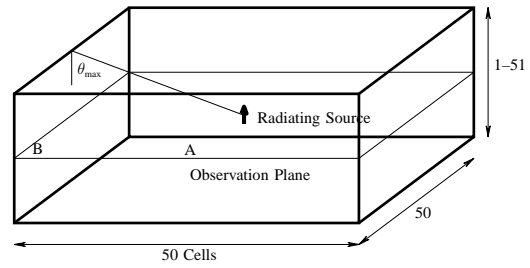

Fig. 1. PML test domain with the PML regions removed for clarity. Observed reflections are mainly due to side walls, except when the z-dimension approaches one cell where steep reflections off the top and bottom walls dominate. Radiating source and observation points A and B are located at (25,25), (25,0) and (0,0), respectively, within the observation plane.
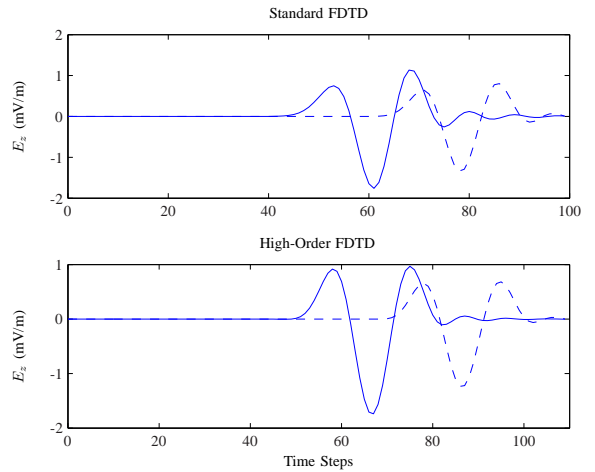

Fig. 2. Observed field values at locations A (solid) and B (dashed) which verify sufficient wave interaction with the PML layer for parameter optimization purposes.

and what is left of it re-enters the test domain at $n = 95$. Once each simulation is completed, E_z data are collected from the central xy-plane (observation plane in Fig. 1) and introduced to the optimization routine.

Most PML reflection errors observed from the above experimental setup will be due to reflections corresponding to incidence angles $\theta \leq \theta_{\max} = \pi/2$ within the observation plane. This $\theta_{\max}$ value also holds for the normal plane as all six PML interfaces are equidistant from the centrally located point source. When the z-dimension of the test vacuum is collapsed, however, $\theta_{\max}$ that corresponds to the top and bottom PML interfaces will start to increase beyond $\pi/4$, reaching $86.6°$ when the test vacuum is collapsed to $50 \times 50 \times 1$ FDTD cells. For the rest of this work, $\theta_{\max}$ will refer to this increasing maximum incidence angle as the vaccuum's z-dimension is collapsed as illustrated in Fig. 1. This relatively rough experimental setup is deliberately chosen as it closely mimics real-world simulation challenges, especially when modeling electrically large structures.

In the following section, two sets of optimized PML parameters will be derived for each combination of FDTD algorithms and PML formulations; one set from a $50 \times 50 \times 51$-cell setup an another from a $50 \times 50 \times 1$-cell setup that highlights the near-grazing angle wave incidence challenge. To test each set of optimized PML parameters, it will be inserted back in the test setup and the error function defined earlier will be collected from a series of simulations where the z-dimension is collapsed incrementally, sweeping in the process the range $\pi/4 \leq \theta_{\max} \leq 87°$.

IV. OPTIMIZATION RESULTS AND COMPARATIVE ANALYSIS

Table 1 summarizes the derived PML parameters from the optimization process detailed in the previous section for the standard and high-order FDTD algorithms. Listing the PML parameters in the table to 4–5 significant digits is necessary for optimum performance. For example, the -175 dB reflection error increased by 5 dB when the corresponding parameters were implemented with only two significant digits. Furthermore, experimenting with several sets of initial guesses was necessary to achieve minimal reflection error levels, especially with convolutional PML optimization runs.

Table 1. Optimized $\underline{S}$plit-field, $\underline{U}$niaxial and $\underline{C}$onvolutional PML profiles for conventional and wide - angle wave incidence on a 10-layer PML. (Units: S/m for σ and dB for error function Ψ)

		Standard FDTD		High-Order FDTD	
	$\theta_{\max}$	45°	87°	45°	87°
S	$\sigma_{\max}$	0.6108	0.8051	0.8466	0.6469
	n_σ	3.9849	5.5968	3.6958	5.4837
	Ψ	-158	-116	-157	-119
U	$\sigma_{\max}$	0.3532	0.4413	0.4526	0.4836
	n_σ	3.1769	3.9540	3.2428	4.1050
	Ψ	-152	-128	-151	-127
C	$\sigma_{\max}$	0.3338	0.3226	0.5132	0.4288
	n_σ	4.1322	3.2352	3.3551	2.9732
	$\kappa_{\max}$	0.3414	0.3207	0.4196	0.4699
	n_κ	3.8151	4.7704	2.8402	3.6169
	$a_{\max}$	0	0.0980	0	0.0822
	n_a		1.0145		1.1934
	Ψ	-175	-148	-157	-147

A. Optimized PML Parameters at $\theta_{max} = \pi/4$

These parameters are most suitable for electrically small problems where the bulk of outgoing energy can be made to impinge on the surrounding PML regions within the limits of $\theta_{\max} = \pi/4$ without incurring significant

computational burden. We can deduce from tabel 1 that for standard FDTD, split-field PML performs slightly better than uniaxial PML (6 dB lower reflection) due to its more favorable $\sigma_{\max}$ and n_σ combination. Both however are vastly outperformed by convolutional PML with a 17 dB margin over split-field PML. The performance of the optimized parameters for the high-order FDTD algorithm mimicked those of standard FDTD for both split-field and uniaxial PML formulations. Convolutional PML, on the other hand, failed to match its excellent performance with standard FDTD and managed only to match split-field PML permanence which was the same for both FDTD algorithms. It should be noted here that for all cases in Table 1, the optimization process maintained $0.3 < \kappa_{\max} < 0.5$ which justifies the slight deviation from previous convolutional PML implementations mentioned at the end of Section II.

Figure 3 charts the performance of the optimized PML parameters at $\theta_{\max} = \pi/4$ when the test domain's z-dimension is gradually collapsed, sweeping $\theta_{\max}$ from $\pi/4$ to $87°$. Standard FDTD curves show that as the incidence angle increases, the clear convolutional PML advantage quickly diminishes and it slightly underperfoms both split-field and uniaxial PML for the range $65° < \theta_{\max} < 85°$. The high-order FDTD curves of Fig. 3 demonstrate that the three PML variants achieve better wide-angle performances as they stay below, say, -140 dB up to $\theta_{\max} \approx 80°$, compared to standard FDTD's $\theta_{\max} \approx 75°$.

B. Optimized PML Parameters at $\theta_{max} = 87°$

When the PML parameters were optimized at the extreme incidence angle $\theta_{\max} = 87°$ to best accommodate electrically large models, both standard and high-order FDTD algorithms produced comparable performances across each of the three PML variants as shown in Table 1. On the other hand, there were clear differences among the PML formulations, as uniaxial and convolutional PML afforded roughly 10 dB and 30 dB lower reflection errors, respectively, than split-field PML. As the incidence angle is swept though $\pi/4 < \theta_{\max} < 87°$ (see Fig. 4), all three PML variants more or less maintained flat response. The convolutional PML formulation in particular shows superior extreme angle composure as well as lower overall levels than the other two formulations for both FDTD algorithms. While the reflection error levels in this figure do not match those of Fig. 3, they do represent reliable wide-angle PML performances. Depending on the problem under study, these error levels could be controlled by varying the PML depth d and re-running the optimization routine.

C. Frequency Response of Optimized PML Parameters

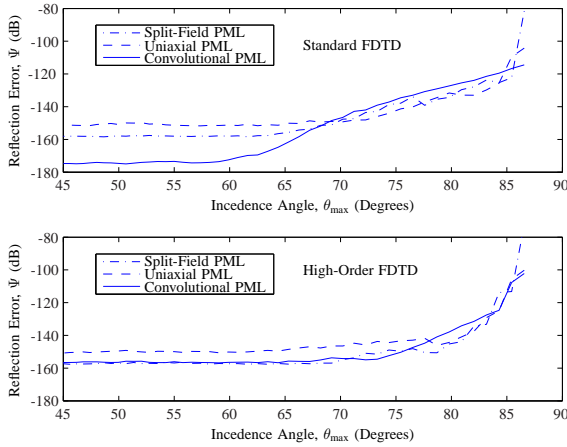To verify that the optimized PML parameters are insensitive to small frequency variations, the detailed

Fig. 3. Comparative wide-angle performance of the three PML formulations when optimized at $\theta_{\max} = \pi/4$.
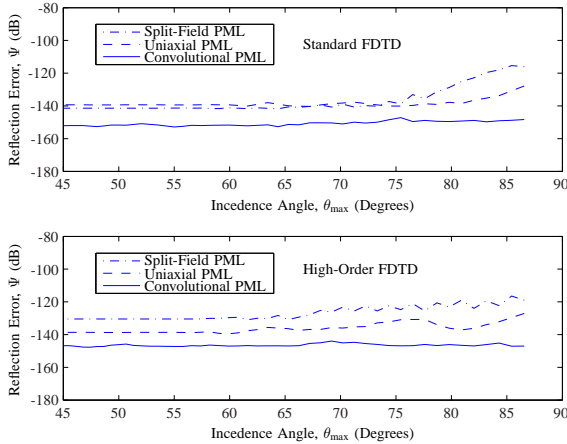

Fig. 4. Comparative wide-angle performance of the three PML formulations when optimized at $\theta_{\max} = 87°$.

experiment in Section III was repeated for convolutional PML and standard FDTD with a unit impulse source replacing equation (19) within a test domain sized $50 \times 50 \times 1$. Two sets of optimized PML parameters, at $\theta_{\max} = \pi/4, \ 87°$, were tested and compared in the power spectral density plots of Fig. 5. (The 100-step time series data were collected at points A and B, marked in Fig. 1.) This comparison illustrates maintained minimal reflection errors except at the frequency range where the spatial grid becomes too coarse to support accurate FDTD simulations. (It should be remembered here that the FDTD grid was designed around 20 cells per wavelength at 1 GHz.)

In gerneral, however, PML parameters are frequency dependent. For example, when the 3-harmonics source of equation(19) was driven with a 60 GHz fundamental, the optimization routine produced $\sigma_{\max} = 38.6781$ S/m and $n_\sigma = 3.7181$ at $\theta_{\max} = \pi/4$ for the split-field PML and standard FDTD, with the same -158 dB error level as in Table 1.
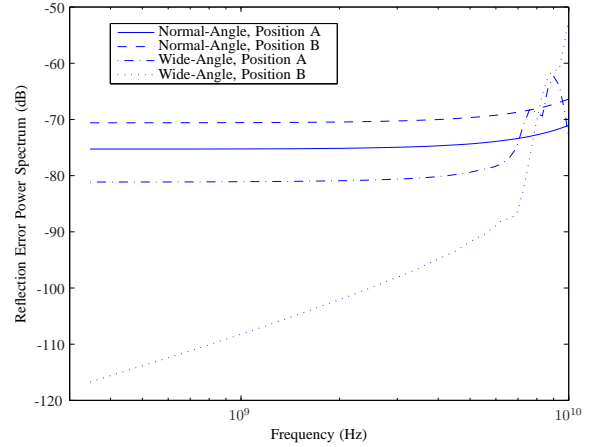

Fig. 5. Reflection errors' frequency response of convolutional PML with standard FDTD using normal-angle and wide-angle PML parameters optimized at $\theta_{\max} = \pi/4$ and $87°$, respectively.

V. CONCLUSION

This work demonstrated that the three main PML variants, Bérenger's original split-field PML, the uniaxial PML and the convolutional PML, are all capable of good outgoing wave absorbing capabilities at near grazing angles. This capability was tested in three-dimensional simulations up to $87°$ incidence angles. The developed optimization process provided different sets of PML parameters depending on how wide an incidence angle is anticipated. This wide-angle performance comes at the expense of reduced absorption capabilities at near normal wave incidence. However, the far more critical advantage of this extreme wide-angle capability is the elimination of the need for prohibitively large scatterer/PML buffer zones when modeling electrically large structures.

Both low-order (standard) FDTD and a high-order FDTD algorithm were tested and optimized for near-normal and near-grazing PML performances. When both were optimized for near-normal incidence angles, the high-order FDTD algorithm demonstrated wider-angle capabilities than standard FDTD, providing flat absorption response across $0 \leq \theta \leq 80°$ compared to standard FDTD's $0 \leq \theta \leq 75°$. Of the three PML variants, the convolutional PML formulation demonstrated best wide-angle capabilities. The optimized PML parameters in this work, though frequency dependent in general, were shown to be insensitive to small frequency variations. Optimized PML parameters could be easily implemented in existing FDTD codes with no code changes or added computational burden.

ACKNOWLEDGMENT

REFERENCES

[1] J. Fang, "Time domain finite difference computation for Maxwell's equations," Ph.D. dissertation, University of California at Berkeley, Berkeley, CA, 1989.

[2] M. F. Hadi and M. Piket-May, "A modified FDTD (2,4) scheme for modeling electrically large structures with high-phase accuracy," *IEEE Trans. Antennas Propagat.*, vol. 45, no. 2, pp. 254–264, Feb. 1997.

[3] E. Turkel and A. Yefet, "Fourth order method for Maxwell's equations on a staggered mesh," vol. 4, pp. 2156–2159, Jul. 1997.

[4] J. B. Cole, "A high-accuracy realization of the Yee algorithm using non-standard finite differences," *IEEE Trans. Microwave Theory Tech.*, vol. 45, no. 6, pp. 991–996, Jun. 1997.

[5] J. L. Young, D. Gaitonde, and J. S. Shang, "Toward the construction of a fourth-order difference scheme for transient EM wave simulation: Staggered grid approach," *IEEE Trans. Antennas Propagat.*, vol. 45, no. 11, pp. 1573–1580, Nov. 1997.

[6] G. J. Haussmann, "A dispersion optimized three-dimensional finite-difference time-domain method for electromagnetic analysis," Ph.D. dissertation, University of Colorado at Boulder, Boulder, CO, 1998.

[7] N. V. Kantartzis and T. D. Tsiboukis, "A higher-order FDTD technique for the implementation of enhanced dispersionless perfectly matched layers combined with efficient absorbing boundary conditions," *IEEE Trans. Magn.*, vol. 34, no. 5, pp. 2736–2739, Sep. 1998.

[8] Y. W. Cheong, Y. M. Lee, K. H. Ra, J. G. Kang, and C. C. Shin, "Wavelet-Galerkin scheme of time-dependent inhomogeneous electromagnetic problems," *IEEE Microwave Guided Wave Lett.*, vol. 9, no. 8, pp. 297–299, Aug. 1999.

[9] E. A. Forgy and W. C. Chew, "A time-domain method with isotropic dispersion and increased stability on an overlapped lattice," *IEEE Trans. Antennas Propagat.*, vol. 50, no. 7, pp. 983–996, Jul. 2002.

[10] H. E. Abd El-Raouf, E. A. El-Diwani, A. Ammar, and F. El-Hefnawi, "A low-dispersion 3-D second-order in time fourth-order in space FDTD scheme ($m3d_{24}$)," *IEEE Trans. Antennas Propagat.*, vol. 52, no. 7, pp. 1638–1646, Jul. 2004.

[11] M. F. Hadi, "A finite volumes-based 3-D low dispersion FDTD algorithm," *IEEE Trans. Antennas Propagat.*, vol. 55, no. 8, Aug. 2007.

[12] M. F. Hadi and R. K. Dib, "Eliminating interface reflections in hybrid low-dispersion FDTD algorithms," *Appl. Computat. Electromag. Soc. J.*, vol. 22, no. 3, pp. 306–314, Nov. 2007.

[13] ——, "Phase-matching the hybrid FV24/S22 FDTD algorithm," *Progress in Electromagnetics Research*, vol. 72, pp. 307–323, 2007.

[14] A. M. Shreim and M. F. Hadi, "Integral PML absorbing boundary conditions for the high-order M24 FDTD algorithm," *Progress in Electromagnetics Research*, vol. 76, pp. 141–152, 2007.

[15] J.-P. Bérenger, "A perfectly matched layer for the absorption of electromagnetic waves," *Journal of Computational Physics*, vol. 114, no. 2, pp. 185–200, 1994.

[16] W. C. Chew and W. H. Weedon, "A 3D perfectly matched medium from modified Maxwell's equations with stretched coordinates," *Microwave Opt. Technol. Lett.*, vol. 7, no. 13, pp. 599–604, Sep. 1994.

[17] Z. S. Sacks, D. M. Kingsland, R. Lee, and J.-F. Lee, "A perfectly anisotropic absorber for use as an absorbing boundary condition," *IEEE Trans. Antennas Propagat.*, vol. 43, no. 12, pp. 1460–1463, Dec. 1995.

[18] S. D. Gedney, "An anisotropic perfectly matched layer-absorbing medium for the truncation of FDTD lattices," *IEEE Trans. Antennas Propagat.*, vol. 44, no. 12, pp. 1630–1639, Dec. 1996.

[19] M. Kuzuoglu and R. Mittra, "Frequency dependence of the constitutive parameters of causal perfectly matched anisotropic absorbers," *IEEE Microwave Guided Wave Lett.*, vol. 6, no. 12, pp. 447–449, Dec. 1996.

[20] J. A. Roden and S. D. Gedney, "Convolution PML (CPML): An efficient FDTD implementation of the CFS-PML for arbitrary media," *Microwave Opt. Technol. Lett.*, vol. 27, no. 5, pp. 334–339, Dec. 2000.

[21] J.-P. Bérenger, "Numerical reflection from FDTD-PMLs: A comparison of the split PML with the unsplit and CFS PML," *IEEE Trans. Antennas Propagat.*, vol. 50, no. 3, pp. 258–265, Mar. 2002.

[22] S. C. Winton and C. M. Rappaport, "Specifying PML conductivities by considering numerical reflection dependencies," *IEEE Trans. Antennas Propagat.*, vol. 48, no. 7, pp. 1055–1063, Jul. 2000.

[23] Y. S. Rickard and N. K. Georgieva, "Problem-independent enhancement of PML ABC for the FDTD method," *IEEE Trans. Antennas Propagat.*, vol. 51, no. 10, pp. 3002–3006, Oct. 2003.

[24] S. Kim and J. Choi, "Optimal design of PML absorbing boundary conditions for improving wide-angle reflection performance," *Electron. Lett.*, vol. 40, no. 2, pp. 104–105, Jan. 2004.

[25] X. L. Travassos, S. L. Avila, D. Prescott, A. Nicolas,

and L. Krähenbühl, "Optimal configurations for perfectly matched layers in FDTD simulations," *IEEE Trans. Magn.*, vol. 42, no. 4, pp. 563–566, Apr. 2006.

[26] N. V. Kantartzis, T. V. Yioultsis, T. I. Kosmanis, and T. D. Tsiboukis, "Nondiagonally anisotropic PML: A generalized unsplit wide-angle absorber for the treatment of the near-grazing effect in FDTD meshes," *IEEE Trans. Magn.*, vol. 36, no. 4, pp. 907–911, Jul. 2000.

[27] R. Holland, L. Simpson, and K. Kunz, "Finite-difference analysis of EMP coupling to lossy dielectric structures," *IEEE Trans. Electromagn. Compat.*, vol. EMC-22, no. 3, pp. 203–209, Aug. 1980.

[28] A. Taflove and S. Hagness, *Computational Electrodynamics: The Finite-Difference Time-Domain Method, 3 ed.* Boston, MA: Artech House, 2005.

Mohammed Hadi his B.S. degree in electrical engineering from Kuwait University in 1988 and his M.S. and Ph.D. degrees from the University of Colorado at Boulder in 1992 and 1996. Dr. Hadi is an Associate Professor at the Electrical Engineering Department of Kuwait University. His research is currently focused on FDTD development for modeling electrically large structures. He also has over a decade's experience in governmental work and consultations in the areas of engineering training, higher education planning and Kuwait's labour profile studies. Dr. Hadi was a Visiting Research Scholar at Duke University, North Carolina during 2007/08.